African Journal of Advanced Pure and Applied Sciences (AJAPAS)
Online ISSN: 2957-644X
Volume 4, Issue 1, January - March 2025
Page No: 8-18
Website: https://aaasjournals.com/index.php/ajapas/index
ISI 2024: 0.877 **SJIFactor 2024: 6.752** **معامل التأثير العربي: 1.6**

High-Gain Circularly Polarized Rectangular Dielectric Resonator Antenna Array at 28 GHz for Millimeter-Wave Applications

Tarek S. Abdou [1*], Alsayah A. M. Emhemed [2]
[1] Department of Electrical and Electronic Engineering, Higher Institute of Engineering Technology, Tripoli, Libya.
[2] Libyan Authority for Scientific Research, Tripoli, Libya.

هوائي مصفوفة رنان عازل مستطيل عالي الكسب ذو استقطاب دائري عند تردد 28 جيجاهرتز لتطبيقات الموجات المليمترية

طارق صالح عبدو [1*]، السايح علي معتوق امحمد [2]
[1] قسم الهندسة الالكترونية والكهربائية، المعهد العالي للتقنيات الهندسية، طرابلس، ليبيا.
[2] الهيئة الليبية للبحث العلمي، طرابلس، ليبيا.

[*]Corresponding author: tsabdou1@hiett.edu.ly

Received: October 23, 2024	Accepted: December 25, 2025	Published: January 05, 2025

Abstract
This study presents a rectangular dielectric resonator antenna (RDRA) array designed to operate in the 28 GHz millimeter-wave (mmWave) spectrum. It achieves circular polarization (CP) by utilizing an innovative feed network with cross-slots. The DRA's dimensions, relative to the free-space wavelength (λ_o), are $0.478\lambda_o \times 0.478\lambda_o \times 0.28\lambda_o$. The 1 × 4 array demonstrates excellent performance, delivering a substantial broadside gain of 14 dBic at 28 GHz, along with an axial ratio (AR) bandwidth of 13% and an impedance bandwidth of 27.3%. These features position it as a highly promising candidate for a wide range of applications. CST Microwave Studio was used for the entire simulation design process.

Keywords: DRA, cross slot, bandwidth, Array antenna, Axial Ratio.

الملخص
قدم هذه الدراسة مجموعة رائدة من هوائيات الرنان العازل المستطيلة (DRA) مصممة للعمل في طيف الموجات المليمترية (mmWave) بتردد 28 جيجاهرتز. وهي تحقق الاستقطاب الدائري (CP) من خلال الاستفادة من شبكة تغذية مبتكرة ذات فتحات متقاطعة. تبلغ أبعاد هوائي الرنان العازل المستطيلة، فيما يتعلق بطول الموجة في الفضاء الحر ((λ_o، $0.28\lambda_o \times 0.478\lambda_o \times 0.478\lambda_o$. ومن اللافت للنظر أن هذه المجموعة التي يبلغ حجمها 1 × 4 توضح أداءً متميزًا، حيث تقدم مكسبًا يبلغ 14 ديسيبل عند 28 جيجاهرتز، مقترنًا بعرض نطاق محوري بنسبة 13٪ وعرض نطاق معاوقة بنسبة 27.3٪. هذه الميزات تضعها كمرشح واعد للغاية لمجموعة واسعة من التطبيقات .تم تنفيذ جميع عمليات المحاكاة باستخدام برنامج CST microwave studio.

الكلمات المفتاحية: هوائي الرنان العازل، فتحة متقاطعة، عرض النطاق الترددي، هوائي المصفوفة، النسبة المحورية.

Introduction

In recent years, significant advancements have been made in dielectric resonator antenna (DRA) arrays, particularly for millimeter-wave and 5G applications. In [1] introduced a substrate-integrated waveguide (SIW) series-fed DRA array that achieved a high radiation efficiency of over 90%, a gain of 11.7 dB, and a 4.7% bandwidth. To address mounting errors, a substrate-integrated design was proposed in [2], where the resonator and feed were fabricated together on the same printed circuit board, enabling both linear and circular polarization operation at Ka-band. In another study, a polymer-based approach for DRAs was developed, utilizing acrylic templates filled with composite materials this method achieved a 12% bandwidth and a realized gain of 10.5 dBi at 60 GHz [3]. Further improvements appeared with a stacked DRA featuring an enlarged cavity-backed design [4], enhancing the bandwidth to 16.4% (62.7–73.9 GHz) and achieving a gain of 17.2 dBi. Furdermore, artificial

grid DRAs, introduced, embedded metal grid structures to increase the effective permittivity, resulting in a measured gain of 12 dBi, a bandwidth of 6 GHz, and 76% radiation efficiency at 32 GHz [5]. Another advancement [6] addressed performance limitations of conventional printed circuit board antennas for 5G networks, developing a 64-element DRA array to support the high data rates and low latency required for fixed wireless systems. The most recent work, outlined in [7], focused on fully integrated DRAs (FIDRAs) using electromagnetic band-gap structures. This design achieved an 11.5% bandwidth (29.6–33.2 GHz) and a peak gain of 7.85 dBi, with added multi-beam array capabilities. These advancements collectively underscore the growing potential of DRAs for achieving higher bandwidth, improved gain, and enhanced integration in next-generation wireless communication systems.

This study aims to enhance the gain, improve circular polarization performance, and achieve a wide bandwidth in dielectric resonator antennas (DRAs). By exploring innovative design techniques and integrating advanced materials, the objective is to optimize antenna efficiency, broaden operational bandwidth, and effectively utilize high-order modes to address key challenges in 5G and next-generation wireless communication networks, as well as millimeter-wave applications.

Design Methodology

The methodology began with identifying the supported modes of the DRA to ensure optimal performance at 28 GHz, selected for its relevance to mmWave applications requiring high data rates, low latency, and reliable connectivity. A single DRA element was designed using a dielectric material with appropriate permittivity to balance size, efficiency, and bandwidth by using CST microwave studio. The geometry and dimensions were optimized through simulations for mode excitation and impedance matching, and a feeding mechanism, such as a microstrip line, was integrated to excite the resonant mode. Simulations confirmed the single element's compliance with requirements for low profile, wideband operation, and high radiation efficiency. Based on this, a DRA array was developed to enhance gain and achieve directional radiation, with elements strategically arranged to maximize constructive interference and improve directivity.

Supported modes of Rectangular DRA.

The resonance frequency of TEmnp modes in DRA can be found using the dielectric waveguide model (DWM) [8].

$$k_x = \frac{m\pi}{a} \quad (1)$$

$$k_y = \frac{n\pi}{b} \quad (2)$$

$$k_z \tan\left(\frac{k_z h}{2}\right) = \sqrt{\left((\varepsilon_r - 1)k_0^2 - k_x^2\right)} \quad (3)$$

$$k_x^2 + k_y^2 + k_z^2 = \varepsilon_r k_0^2 \quad (4)$$

$$k_0 = \frac{2\pi}{\lambda_0} = \frac{2\pi f_0}{c} \quad (5)$$

In this case, λ_0 indicates the wavelength in open space, while c is the speed of light. Consequently, it is possible to identify the resonant frequency modes as:

$$f_0 = \frac{c}{2\pi\varepsilon_r}\sqrt{\left(k_x^2 + k_y^2 + k_z^2\right)} \quad (6)$$

Furthermore, the DRA dimensions a, b, and *h* can be used to characterise the RDRA's magnetic field distribution as follows.

$$H_z = \frac{(k_z k_x)}{(jw\mu_0)} \sin(k_x x)\cos(k_y y)\sin(k_z z) \quad (7)$$

$$H_y = \frac{(k_y k_x)}{(jw\mu_0)} \sin(k_x x)\sin(k_y y)\cos(k_z z) \quad (8)$$

$$H_x = \frac{(k_y^2 + k_z^2)}{(jw\mu_0)} \cos(k_x x)\cos(k_y y)\cos(k_z z) \quad (9)$$

$$E_x = 0 \quad (10)$$

$$E_y = k_z \cos(k_x x)\cos(k_y y)\sin(k_z z) \quad (11)$$

$$E_z = -k_y \cos(k_x x)\sin(k_y y)\sin(k_z z) \quad (12)$$

When a rectangular Dielectric Resonator Antenna is placed on a ground plane, the excitation of transverse magnetic (TM) modes becomes impossible. This limitation arises because TM modes require the electric field (E-field) to have maximum intensity at z = 0, a condition that conflicts with the boundary conditions at the ground plane. Furthermore, the resonance frequency of both transverse electric and transverse magnetic modes depends on the dimensions and permittivity of the DRA. This dependency highlights the complex interplay between the antenna's physical properties and its electromagnetic performance. Recognizing these constraints is essential for designing DRAs tailored to specific applications, balancing practical requirements with theoretical principles. In addition, the higher-order modes of TE_{113}, TE_{133} were simultaneously excited at 28 GHz and 30.5 GHz, respectively.

Single DRA Element

The antenna configuration is depicted in Figure 1, which also includes the dielectric constants and loss tangents for the DRA and substrate, which are $\varepsilon r = 9.9$ with $\tan\delta < 0.0001$ and $\varepsilon s = 3.66$ with $\tan\delta = 0.0027$, respectively. These are the RDRA dimensions: $l = w = 5.3$ mm and $h = 3$ mm. These dimensions were determined using the dielectric waveguide model (DWM) and the CST Eigenmode solver, which were utilized to calculate the resonance frequencies of the TEmnp modes. The substrate has overall dimensions of $L = 20$ mm, $W = 20$ mm, and hs = 0.245 mm. A 50Ω microstrip line was used to feed the cross-slot. The lengths and widths of the cross-slot arms play a critical role in optimizing the impedance and axial ratio (AR) bandwidths. [9]. In order to generate circularly polarised (CP) radiation, unequal arm lengths were chosen [9]. The first and second cross-slot arms' lengths were optimised to be 1.7 mm and 3.2 mm, respectively, and they had the same width of 0.35 mm. The initial widths and lengths of the slots can be found using the formulas:

$$l_s = \frac{0.4\lambda_0}{\sqrt{\varepsilon_e}} \quad (13)$$

$$\varepsilon_e = \frac{\varepsilon_r + \varepsilon_s}{2} \quad (14)$$

$$w_s = 0.2 l_s \quad (15)$$

where εr and εs stand for the substrate and DRA's respective dielectric constants. The best place to start the stub length l_{stub} is :

$$l_{stub} = \frac{\lambda_g}{4} \quad (16)$$

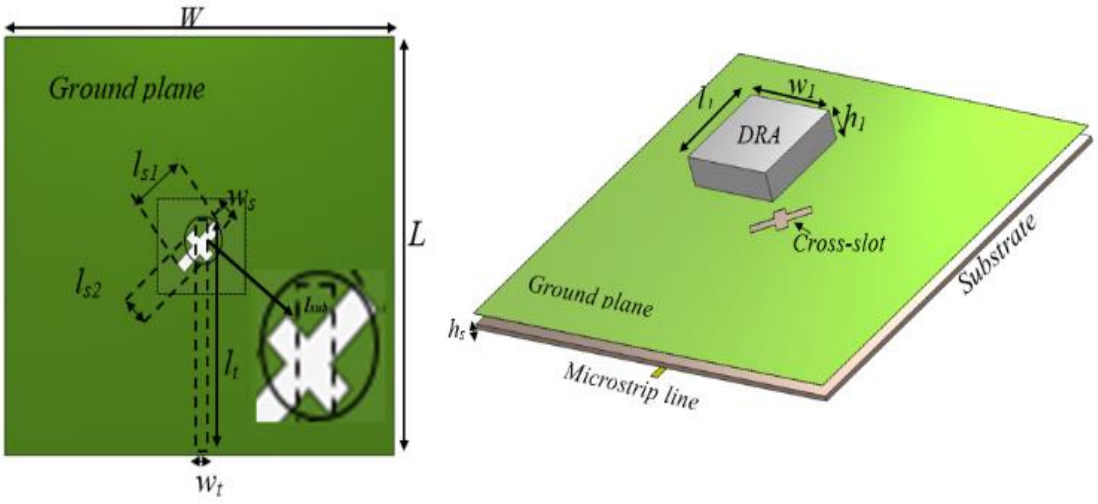

Figure 1: The proposed single DRA.

Particular care was taken to select the DRA's minimum height while preserving acceptable radiation properties. The impedance bandwidth of a rectangular dielectric resonator antenna (DRA) is not directly correlated with its height, as Figure 2 illustrates for various DRA heights.

Instead, it's influenced by various factors like the dielectric material properties, resonant frequency, and the resonator's dimensions. The impedance bandwidth is typically associated with the resonant frequency and the size of the resonator, rather than solely with its height. Validating the selected dimensions in the case study involves assessing whether the chosen dimensions align with the desired resonant frequency and the associated impedance bandwidth. If the dimensions lead to the intended resonant frequency and the desired impedance bandwidth, it would confirm the suitability of the chosen dimensions for the application. This validation ensures that the antenna meets the required performance criteria. Figure 3 illustrates the broadside gain, clearly demonstrating that the maximum gain of approximately 9 dBic was achieved at 28 GHz with a height of 3 mm. Figure 4 presents the axial ratio, where at a height of 3 mm, circularly polarized (CP) radiation was successfully obtained, delivering a 3 dB axial ratio (AR) bandwidth of 16%.

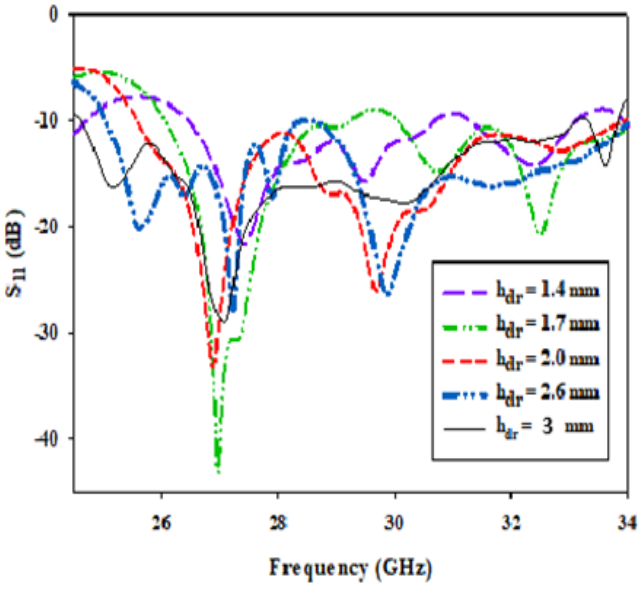

Figure 2: Reflection coefficient of various heights.

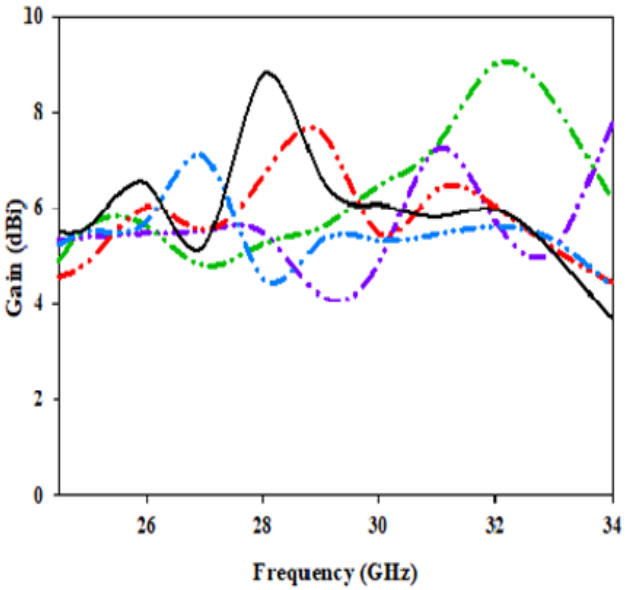

Figure 3: Gains of different heights.

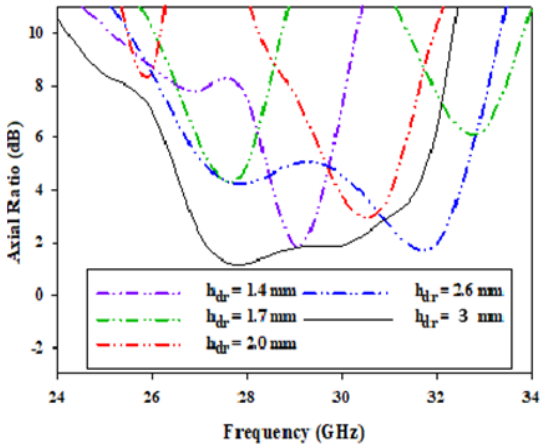

Figure 4: Axial ratio with different heights.

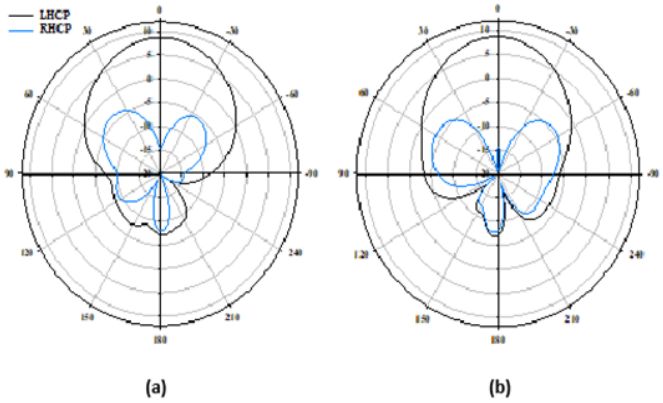

Figure 5: (a) E- Plane and (b) H- Plane radiation 28 GHz.

As explained in Figure 5, Since EL is roughly 20dB higher than ER, the far-field (polar view) patterns at the target frequency 28GHz at DRA height 3 mm demonstrate that the DRA emits a right-hand circular polarisation (LHCP) wave. Though it has a high gain and a significantly wideband operation, the suggested DRA has the lowest profile of the designs that have been published. Table 1displays the final optimal antenna settings.

Table 1: Parameters of the proposed individual DRA element.

Parameter	***L***	***W***	h_s	w_{dr}	l_{dr}	h_{dr}	l_t	w_t	l_{stub}	L_{s1}	L_{s2}	w_s
Value (mm)	20	20	0.254	5.3	5.3	3	10.5	0.45	1	1.7	3.2	0.35

Where L is the ground plane length, W is the width, hs is the substrate height, wdr is the DRA width, ldr is the DRA length, hdr is the DRA height, lt is the microstrip line length, wt is the width, lstub is the stub length, ls1 is the first slot length, ls2 is the second slot length, and ws is the cross slot width.

Array Factor

Assume that each pair of neighboring elements in the array has a d-space between them and that the array has N elements. Furthermore, a complicated current $I_o e^{jn\varphi}$, where $0 < n < N-1$, is used to drive each element. This shows that the antennas have identical current amplitudes and linear phase changes of φ between neighboring elements. Thus, this type of antenna is called a phased array. On the other hand, a uniform array is obtained if $\varphi = 0$. The array factor can be obtained by taking into account an array of isotropic elements that are dispersed along the z-axis [10].

$$AF = 1 + e^{j\Upsilon} + e^{j\Upsilon} + \cdots . + e^{j(N-1)\Upsilon} \qquad (17)$$

Where:

$$\Upsilon = (\beta d\cos\theta + \varphi) \qquad (18)$$

The normalised AF form is:

$$(AR)_n = \frac{1}{N}\left[\frac{\sin\left(\frac{N}{2}\Upsilon\right)}{\sin\left(\frac{1}{2}\Upsilon\right)}\right] \qquad (19)$$

One can achieve a broadside array when the main beam direction is perpendicular to the array axis. (17) makes it evident that when $\gamma = 0$, the greatest AF is attained. The maximum must be at $\theta = 90°$, therefore (18) becomes (20) when the array axis is along the z direction.

$$\Upsilon = (\beta d\cos\theta + \varphi)|_{\theta=90^0} = \varphi = 0 \qquad (20)$$

Therefore, uniform phase and amplitude must be used to excite the array elements in order to meet the broadside radiation requirements. The radiation pattern in a given plane can be found by multiplying the pattern of each individual element by the array's factor [11].

$$E_{array} = E_{singleelement} \times ArrayFactor \qquad (21)$$

Based on the single DRA element mentioned in the preceding section, DRA arrays with 2, 4, and 8 elements will be created. These arrays will be carefully analyzed to provide a deeper insight into the design process. As shown in Figure 6, the single-element DRA offers the widest bandwidth at 31%, followed by the 4-element array at 28.3%, the 2-element array at 23%, and the 8-element array at 18.7%. Therefore, the single element demonstrates superior performance over a broader frequency range compared to the multi-element arrays.

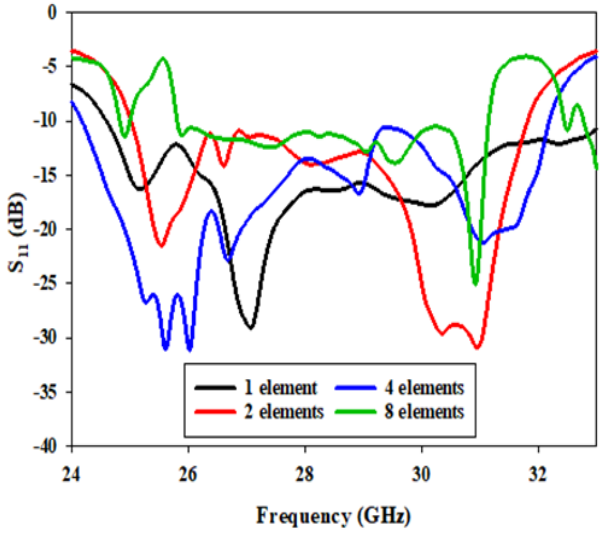

Figure 6: Reflection coefficients of different DRA arrays.

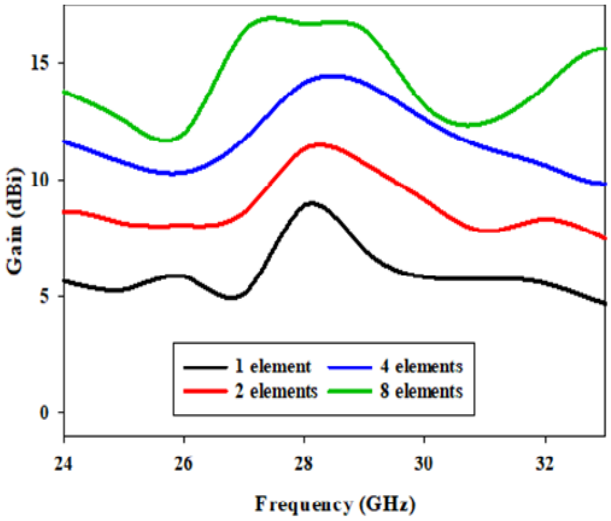

Figure 7: Gain of different DRA arrays.

Figure 7 illustrates the connection between an antenna's gain and element count. Specifically, the gain of the antenna rises with the number of elements. A two-element antenna has a gain of 11.1 dBi, whereas a single-element antenna has a gain of 8.71 dBi. The gain of eight-element antennas is 16.7 dBi, while that of four-element antennas is 14 dBi. This is because a radiation pattern with more elements can be more directed and focussed, resulting in less energy radiating in undesirable directions.

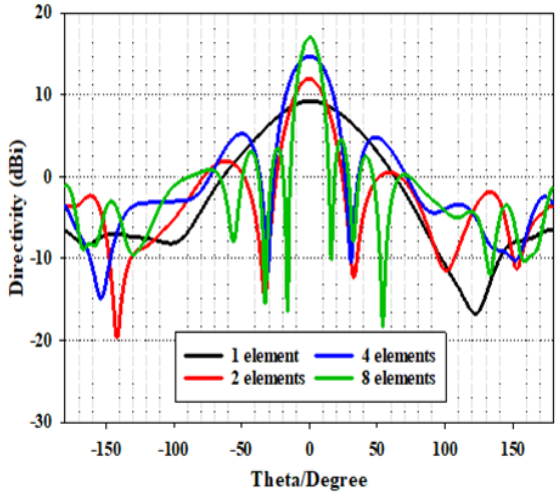

Figure 8: Directivity of different DRA arrays.

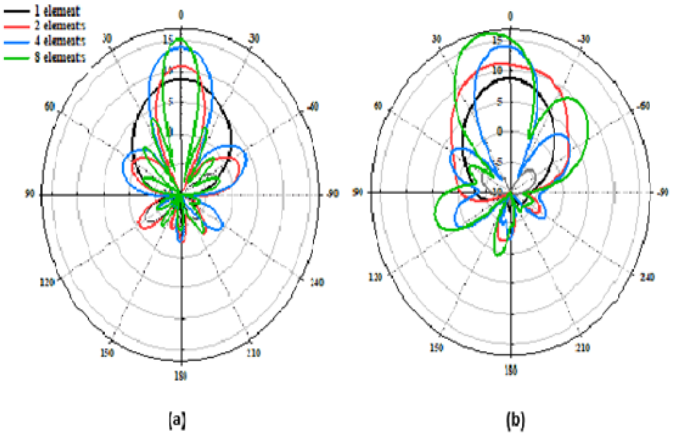

Figure 9: (a) E-plane. (b) H-plane at 28GHz.

Figure 8 shows that the directivity of a 2-element array is 12 dBi, that of a 4-element array is 14.7 dBi, and that of an 8-element array is 17 dBi. The result was a single DRA element, D = 9.25 dBi. This demonstrates how the directivity rises as the number of elements in the array increases, improving the ability to regulate the radiation's direction **[12].**

$$G = \eta \times D \qquad (22)$$

Where gain, efficiency, and directivity are denoted by G, η, and D, respectively.
The radiation pattern at the target frequency of 28 GHz is shown in Figure 9, which makes it abundantly evident that a more element-rich antenna array generates a narrower beam with better gain (directivity).In general, increasing the number of antenna elements leads to an improvement in gain. Table 2 presents the results of the array analyses.

Table 2: Size, gain, and bandwidth of different DRA arrays

Parameter	Single Element	2 Elements	4 Elements	8 Elements
Bandwidth (%)	31	23	28	18.7
Gain (dBi)	8.71	11.1	14	16.6
Size (mm^3)	19 × 21 × 3	35 × 35 × 3	36.5 × 36.5 × 2.93	40 × 45 × 3

1 x 4 DRA Elements.
The single DRA element that was displayed was used to design a compact broadside 4-element array. It was then positioned on a ground plane measuring L = 35 mm, W = 49 mm, on which the cross-slots were etched, as illustrated in Figure 10.

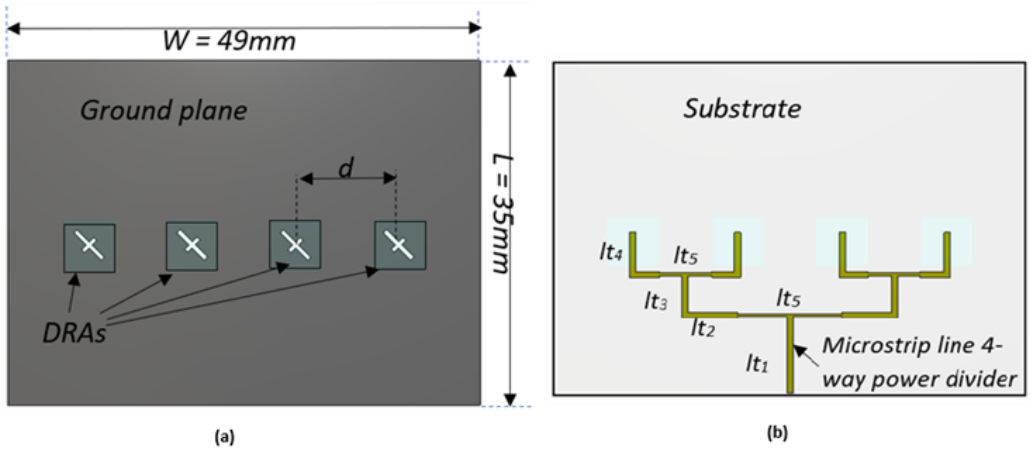

Figure 10: the proposed DRA array

Since a linear array shape provides a more compact structure, it was selected, as shown in Figure 10(a). For the array feed network, a four-way microstrip power divider line was employed., as shown in Figure 10(b), which displays the feed network. The measurements were selected to meet the uniform power division and phase dispersion requirements of the broadside array architecture. Furthermore, two microstrip line widths were selected for characteristic impedances of 50 and 100, respectively: w_{t1} = 0.6 mm and w_{t2} = 0.3 mm. Additionally, the microstrip line portions' lengths were optimised as l_{t1}= 8.25mm, l_{t2} = 5.66 mm, l_{t3} = 4.46 mm, l_{t4} = 4.77 mm, and l_{t5} = 10.7 mm in order to achieve the widest impedance bandwidth.

Results and discussion
Figure 11 displays the simulated reflection coefficient of a single DRA element with impedance bandwidths of about 29%. Additionally, the axial ratio of 13% and the maximum simulated gain of 8.7 dBic at 28 GHz are shown in Figure 12. The simulated E- and H-plane radiation patterns at 28 GHz are shown in Figure 13. A right-hand circularly polarised (RHCP) wave is emitted by the antenna.

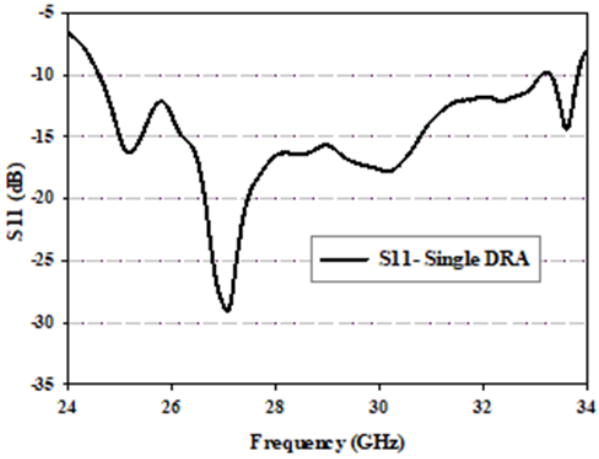

Figure 11: The Reflection Coefficient of Single DRA.

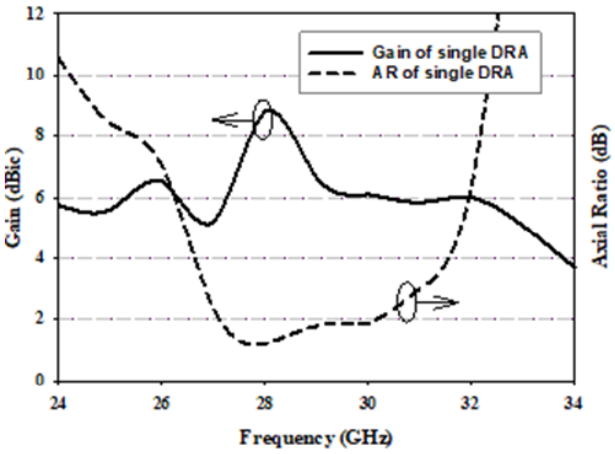

Figure 12: Gain and Axial Ratio of single DRA.

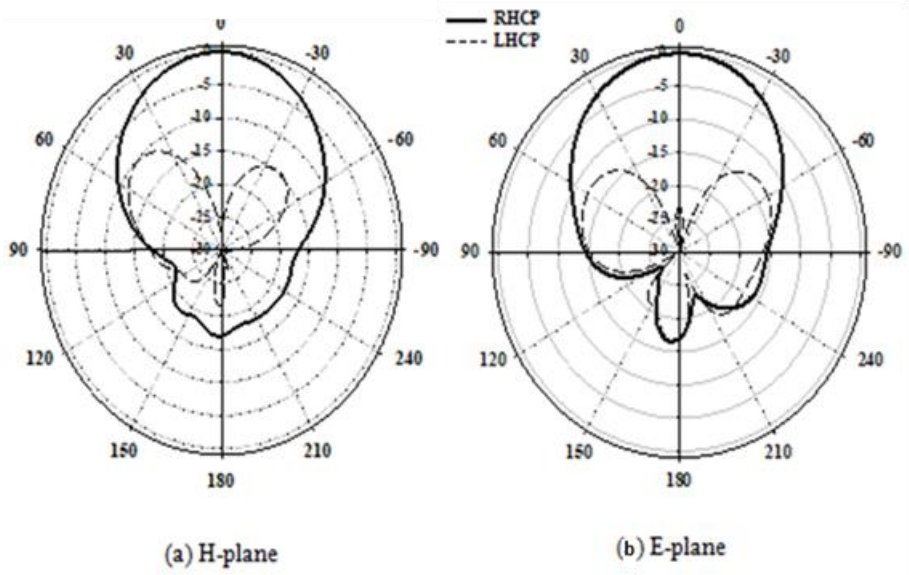

Figure 13: E- and H-planes radiation patterns at 28 GHz

The study thoroughly examined the influence of the separation distance (d) between adjacent Dielectric Resonator Antenna (DRA) elements, as shown in Figure 12. For this investigation, the separation was set at 10 mm [13] , corresponding to one free-space wavelength λo at 28 GHz. Figure 14 shows that this particular spacing yielded the largest impedance bandwidth, measured at 27.3%. This value closely mirrors the performance of a single DRA element, with the improvement attributed to the reduced mutual coupling between the elements at this optimal distance. Figure 15 presents the variations in Axial Ratio (AR) and gain relative to the separation distance. The configuration with the chosen distance produced the broadest AR bandwidth, reaching 13%, and the highest gain, approximately 14 dBic. These enhancements are the result of minimized mutual coupling, which significantly improves antenna characteristics. Figure 16 displays the radiation patterns of both the electric (E-field) and magnetic (H-field) fields for varying separations between the elements. The best radiation performance, in terms of pattern stability and efficiency, was achieved when the separation was maintained at this value. This comprehensive analysis demonstrates that the selected separation distance between DRA elements leads to considerable improvements in impedance bandwidth, gain, and radiation characteristics. The reduction in mutual coupling at this specific spacing plays a crucial role in achieving these enhanced performance metrics. This highlights the significance of optimal element spacing in the design and optimization of antenna arrays for advanced communication systems.

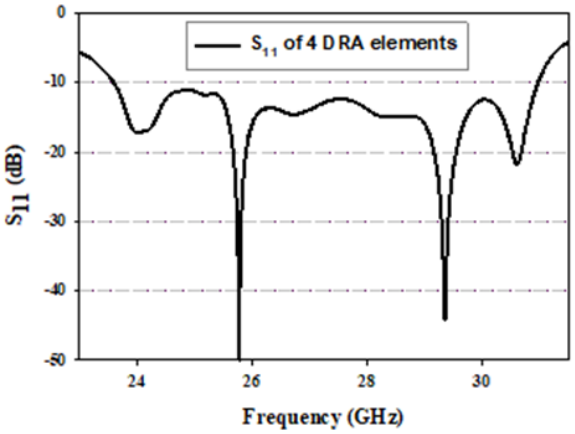

Figure 14: The reflection coefficient of DRA array.

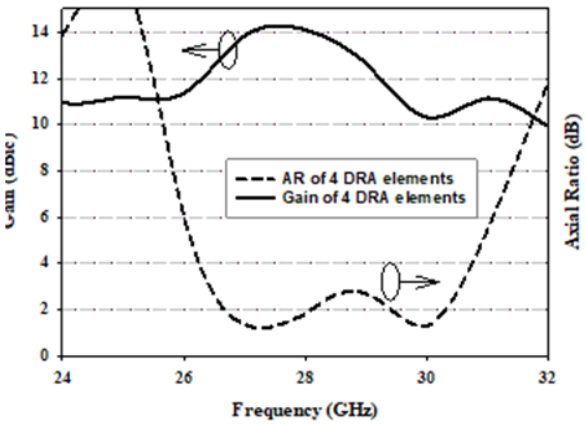

Figure 15: The gain and Axial Ratio of DRA array.

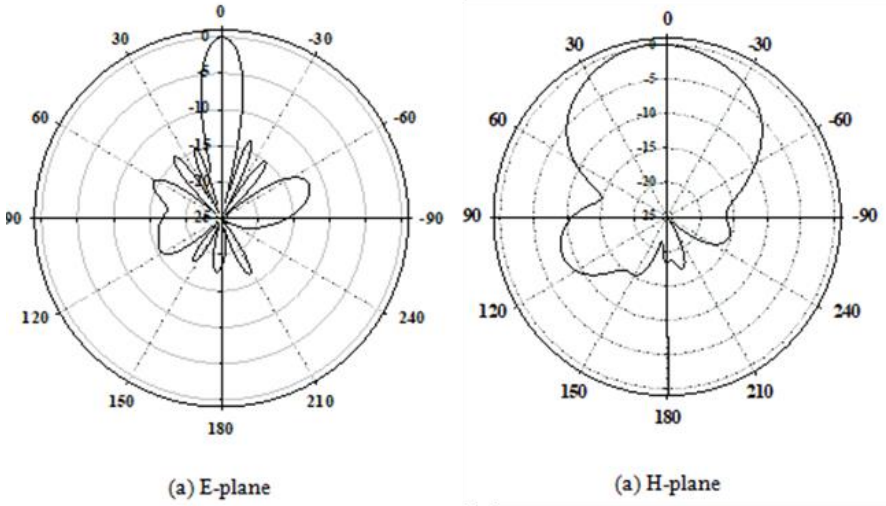

Figure 16: The Normalized radiation pattern of DRA array.

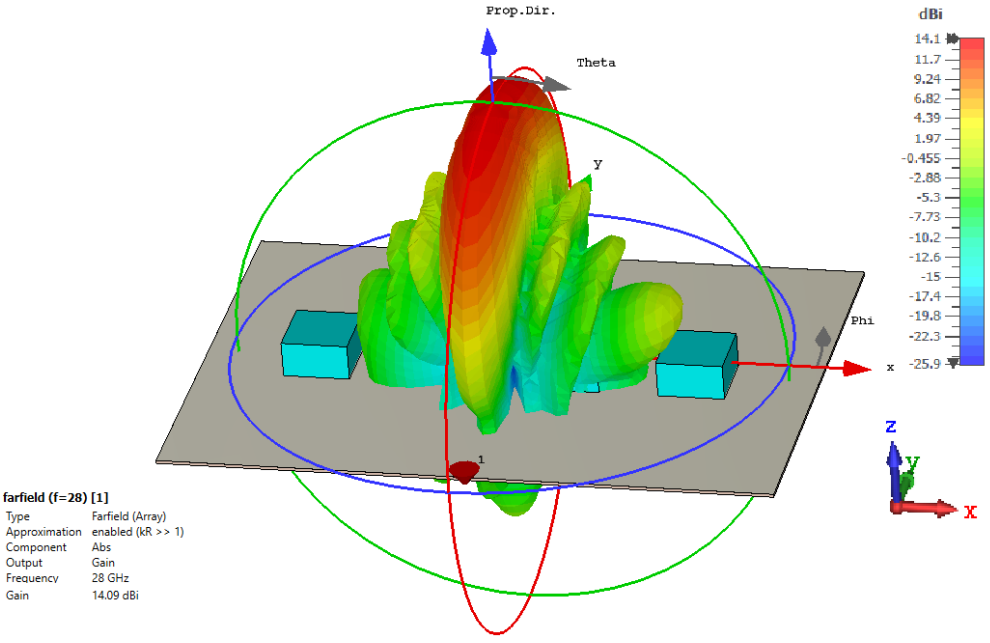

Figure 17: 3D Radiation Pattern of RDRA Array at 28 GHz.

Figure 17 illustrates the 3D far-field radiation pattern of the 1 x 4 DRA array simulated at a frequency of 28 GHz. The figure depicts the gain distribution in dBi using a color gradient, where (red)indicates the regions of maximum gain (up to 14.1 dBi).

Table 3: Evaluation of the proposed antenna's performance in relation to existing designs.

Ref	Bandwidth	AR	Gain	Number of elements
Proposed Array	27.3 %	13 %	14 dBi	1 × 4
[1]	4.7 %	-	11.7 dBi	4 × 1
[2]	-	-	-	2 × 2
[3]	12 %	-	10.5 dBi	4-element
[4]	16.4 %	-	17.2 dBi	4 × 1
[5]	-	-	12 dBi	1 × 4, 1 × 8
[6]	-	-	-	64
[7]	11.5 %	-	7.85 dBi	1 × 4

The results from this study demonstrate significant improvements over the antennas referenced earlier. The antenna achieves a gain of 14 dBi, indicating better signal focusing and directionality. With an S11 of 27%, it shows effective impedance matching and efficient transmission. The axial ratio of 13% suggests a good balance between circular and linear polarization. These performance enhancements are achieved with a compact design of 35 × 49 × 3 mm^3, optimizing the balance between gain, reflection coefficient, and size. Overall, this work advances antenna performance, providing an effective solution for applications that require high-quality signal reception and transmission in limited spaces. The evaluation of proposed array with the previous researches is illustrating in table 3.

Conclusion

A rectangular Dielectric Resonator Antenna (DRA) array, consisting of a 1 x 4 configuration and circularly polarized, is presented in this work for millimeter-wave applications. By utilizing cross-slot coupling and a feeding network, the antenna achieves a radiation efficiency of 93% and an impedance bandwidth of 27.3%, along with an axial ratio of 13%. At 28 GHz, the proposed 1 x 4 RDRA demonstrates a gain of 14 dBic, showing an improvement of 5.3 dBic over a single DRA element. The higher-order modes of the DRA contribute to the enhanced bandwidth and overall performance. The proposed antenna outperforms existing mmWave DRA arrays in both gain and circular polarization bandwidth, making it a promising solution for a variety of applications across different sectors.

References

[1] W. M. Abdel-Wahab, D. Busuioc, and S. Safavi-Naeini, "Millimeter-wave high radiation efficiency planar waveguide series-fed dielectric resonator antenna (DRA) array: analysis, design, and measurements," IEEE Transactions on Antennas and Propagation, vol. 59, no. 8, pp. 2834–2843, 2011.

[2] H. Chu and Y.-X. Guo, "Substrate-integrated dielectric resonator antenna design for Ka-band applications," IEEE Transactions on Antennas and Propagation, vol. 64, no. 4, pp. 1323–1332, 2016.

[3] A. A. Qureshi, D. M. Klymyshyn, M. Tayfeh, W. Mazhar, M. Börner, and J. Mohr, "Template-based dielectric resonator antenna arrays for millimeter-wave applications," IEEE Transactions on Antennas and Propagation, vol. 65, no. 9, pp. 4576–4584, 2017.

[4] Z. Chen, L. Zhang, C. Jiang, and Y. Qian, "Millimeter-wave stacked dielectric resonator antenna with cavity-backed design," IEEE Transactions on Antennas and Propagation, vol. 67, no. 5, pp. 2881–2890, 2019.

[5] W. Mazhar, D. M. Klymyshyn, G. Wells, A. A. Qureshi, M. Jacobs, and S. Achenbach, "Low-profile artificial grid dielectric resonator antenna arrays for mm-wave applications," IEEE Transactions on Antennas and Propagation, vol. 67, no. 7, pp. 4406–4417, 2019.

[6] D. Caratelli, D. H. K. Tsang, D. A. R. Kapsalis, and L. D. DiTrapani, "64-element dielectric resonator antenna array for 5G wireless communications," IEEE Transactions on Antennas and Propagation, vol. 68, no. 6, pp. 4187–4196, 2020.
[7] C. Ma, S. Y. Zheng, Y. M. Pan, and Z. Chen, "Millimeter-wave fully integrated dielectric resonator antenna and its multi-beam application," IEEE Transactions on Antennas and Propagation, vol. 70, no. 8, pp. 6571–6580, 2022.
[8] R. D. Maknikar and V. G. Kasabegoudar, "Circularly polarized cross-slot-coupled stacked dielectric resonator antenna for wireless applications," International Journal of Wireless Communications and Mobile Computing, vol. 1, no. 2, pp. 68-73, 2013.
[9] A. A. Abdulmajid, Y. Khalil, and S. Khamas, "Higher-order-mode circularly polarized two-layer rectangular dielectric resonator antenna," IEEE Antennas and Wireless Propagation Letters, vol. 17, no. 6, pp. 1114-1117, 2018.
[10] C. A. Balanis, Antenna theory: analysis and design. John wiley & sons, 2016.
[11] D. Ehyaie, "Novel approaches to the design of phased array antennas," University of Michigan, 2011.
[12] N. M. Nor, M. H. Jamaluddin, M. R. Kamarudin, and M. Khalily, "Rectangular dielectric resonator antenna array for 28 GHz applications," Progress In Electromagnetics Research C, vol. 63, pp. 53-61, 2016.
[13] T. S. Abdou, R. Saad, and S. K. Khamas, "A Circularly Polarized mmWave Dielectric-Resonator-Antenna Array for Off-Body Communications," Applied Sciences, vol. 13, no. 3, p. 2002, 2023.